Energy Conversion and Management 52 (2011) 335–339

Contents lists available at ScienceDirect

Energy Conversion and Management

journal homepage: www.elsevier.com/locate/enconman

Oxide-based thermoelectric power generation module using *p*-type $Ca_3Co_4O_9$ and *n*-type $(ZnO)_7In_2O_3$ legs

Soon-Mok Choi [a], Kyu-Hyoung Lee [b], Chang-Hyun Lim [a], Won-Seon Seo [a,*]

[a] Korea Institute of Ceramic Engineering and Technology, Seoul 153-801, Republic of Korea
[b] Samsung Advanced Institute of Technology, Yongin 446-712, Republic of Korea

ARTICLE INFO

Article history:
Received 23 March 2009
Received in revised form 16 November 2009
Accepted 5 July 2010
Available online 13 August 2010

Keywords:
Thermoelectric power generation
Module
$Ca_3Co_4O_9$
$(ZnO)_7In_2O_3$

ABSTRACT

This study presents the fabrication of an oxide-based thermoelectric power generation module using layer-structured *p*-type $Ca_3Co_4O_9$ and *n*-type $(ZnO)_7In_2O_3$ legs. The potential for development and effective use of high power density thermoelectric generation system is investigated in terms of its power per area, the temperature conditions, and the number of *p*–*n* couples. The significance of the manufacturing factors including contact between legs and electrodes are discussed. The thermoelectric figure of merit values of the *p*-type and *n*-type legs at 1100 K were $0.55 \times 10^{-4}\,K^{-1}$ and $1.35 \times 10^{-4}\,K^{-1}$, respectively. The maximum power obtained was 423 mW with the 44 *p*–*n* couples module, under the thermal condition of a hot-side temperature of 1100 K and a temperature difference $\Delta T = 673$ K.

1. Introduction

Thermoelectric (TE) research has lately received renewed attention because of its ability to convert waste heat into electricity. Finding materials with sufficient performance at high temperatures in air is a key element in the realization of a TE generator. Degenerate semiconducting metal oxides are considered promising TE materials, especially for high-temperature power generation applications, since they have many advantages such as non-toxicity, thermal stability, and high oxidation resistance [1]. A number of studies have focused on layer-structure TE metal oxides such as CoO_2-based oxides and $(ZnO)_m$–In_2O_3 (m = integer) because of their large power factors and anisotropic TE characteristics along different crystal axes. For example $Ca_3Co_4O_9$ is a misfit-layered oxide, which consists of alternating layers of a distorted CaO–CoO–CaO rock-salt-type layer and a CdI_2-type CoO_2 layer stacked in the *c*-axis direction. The electronic structures of the misfit-layered $Ca_3Co_4O_9$ include two-dimensionally dispersive e_g bands across the Fermi energy, which yields *p*-type conduction in the rock-salt Ca_2CoO_3 subsystem, while the Fermi energy lies in the crystal-field gap of the *d* states in the CoO_2 layer. And the t_{2g} levels further split into another doubly degenerated e'_g levels and a non-degenerated a_{1g} level due to the rhombohedral distortion of the octahedron [2]. For these layer-structure materials, electrical and thermal transport properties, including thermal conductivity (κ), electrical conductivity (σ), and Seebeck coefficient (S), could be enhanced by controlling the microstructure. So the TE performance of $Ca_3Co_4O_9$ has been significantly enhanced by textured structure engineering using hot forging [3] and spark plasma sintering (SPS) [4]. And several studies have reported that in Zn–In-based oxides with layer structures controlled by reactive template grain growth (RTGG) method, the *c*-plane shows a larger TE figure of merit ($Z = S^2\sigma/\kappa$) than the *a*- and *b*-planes [5,6].

In this sense, layer-structure oxides with low dimensional transport are highly promising for use in a TE generator. Many oxides modules and the TE properties of those materials have been reported up to now. For examples, *p*-$Ca_3Co_4O_9$/*n*-$CaMnO_3$ [7,8] module, *p*-$NaCo_2O_4$/*n*-ZnO module [9], *p*-$Ca_3Co_4O_9$/*n*-$LaNiO_3$ module [10], *p*-(Ba, Sr)Pb_3/*n*-NiO module [11] were reported. However, a TE power generation module with layer-structure *p*- and *n*-legs has not been fabricated to date.

Further, layer-structured homologous compounds $(ZnO)_mIn_2O_3$ show interesting thermoelectric properties, as a result of changes in the physical properties obtained by controlling the composition of materials composed of binary compounds [12]. And doping other ions also changes the thermoelectric properties. For examples, Ca doping effectively decreases thermal conductivity at high temperatures [13]. The addition of Al for Zn in the $(ZnO)_mIn_2O_3$ increased both the electrical conductivity and the absolute value of the Seebeck coefficient, leading to a significant improvement in the power factor [14]. Crystal structures can also be modified by the isoelectronic substitution of either divalent or trivalent metal ions for Zn or In ions, respectively. Substitution of Mg^{2+}, Co^{2+} and Y^{3+} gave rise to shrinkage of the *c*-axis and elongation of the *a*-axis of a hexagonal unit cell [12]. Consequently, thermal conductivity can be controlled

* Corresponding author. Tel.: +82 2 3282 2496; fax: +82 2 3282 2470.
E-mail address: wsseo@kicet.re.kr (W.-S. Seo).

0196-8904/$ - see front matter
doi:10.1016/j.enconman.2010.07.005

by this modification. As stated above, layer-structured homologous compounds $(ZnO)_mIn_2O_3$ have been extensively studied as candidates for *n*-type thermoelectric oxide materials. However, a TE power generation module with layer-structured homologous compounds $(ZnO)_mIn_2O_3$ has not been fabricated to date.

2. Experimental procedure

2.1. Preparation of n-type and p-type legs

In this study, *p*-type $Ca_3Co_4O_9$ and *n*-type $(ZnO)_7In_2O_3$ materials were synthesized to form the legs of the module by a conventional solid-state reaction method. $Ca_3Co_4O_9$ powder was prepared using commercial CaO (Alfa Aesar, 99.95%) and Co_3O_4 (Kojundo Chemical Co., 99.9%) powders as starting materials. Specific ratios of the powders were weighed and mixed well using a ball mill. The mixture was heated at 900 °C for 12 h in air for homogenization of the final samples. Before the forming process, 1.5 wt.% polyvinyl alcohol (PVA) was added to the pulverized samples to enhance the forming performance. The powder was compacted by cold isostatic press (CIP) at 2000 bar for 5 min. Then, dense polycrystalline ceramic samples were fabricated by conventional sintering (920 °C for 24 h in air) of the single-phase powder.

$(ZnO)_7In_2O_3$ powder was prepared using commercial ZnO (Kojundo Chemical Co., 99.99%) and In_2O_3 (Kojundo Chemical Co., 99.9%) powders as starting materials. Specific ratios of the powders were weighed and mixed well using a ball mill. The mixture was calcined at 1100 °C for 6 h in air for homogenization of the final samples. The calcined powder was ground by a ball mill and compacted by CIP at 2000 bar for 5 min. Then, dense polycrystalline ceramic samples were fabricated by conventional sintering (1550 °C for 2 h in air) of the single-phase powder.

Finally, *p*-type $Ca_3Co_4O_9$ samples were cut into 15 mm × 15 mm × 27 mm rectangular legs; *n*-type $(ZnO)_7In_2O_3$ sintered bodies were cut into 15 mm × 15 mm × 18 mm rectangular legs. This unique design (with differing lengths of $Ca_3Co_4O_9$ and $(ZnO)_7In_2O_3$ legs) was employed in order to secure the stability of $(ZnO)_7In_2O_3$ at a high-temperature because, unlike the resistivity of $Ca_3Co_4O_9$, that of $(ZnO)_7In_2O_3$ degrades at temperatures over 1000 K. It was possible to maintain the maximum temperature of $(ZnO)_7In_2O_3$ under 1000 K, even when the temperature of the hot-side of the module remained over 1100 K. To compensate for the length difference between the $Ca_3Co_4O_9$ and $(ZnO)_7In_2O_3$ legs, a dummy electrode was applied to the $(ZnO)_7In_2O_3$ section. The electrical conductivity (σ) values of *p*-type $Ca_3Co_4O_9$ and *n*-type $(ZnO)_mIn_2O_3$ were measured by the 4-probe method and Seebeck coefficients (S) were obtained from the slope of the linear relation between ΔV and ΔT, where ΔV is the thermoelectromotive force produced by a temperature difference ΔT. Two Pt–Pt/Rh thermocouples were used to attach to both ends of the rectangle samples to control the temperature, and the temperature gradient in the sample was generated by passing cool pure N_2 through a fine tube. These measurements were carried out in a computer-controlled apparatus (Ozawa Science, Thermoelectric Property Measurement System, model RZ2001i). The κ values were calculated by separate measurements, with differential scanning calorimetry for heat capacity and a laser-flash method for thermal diffusivity. All these measurements were confirmed on more than 10 samples. Values of thermoelectric figure of merit Z for samples calculated from σ, S, and κ are in an agreement within a range of 7%.

2.2. Fabrication of TE modules

Fig. 1 shows a photograph of the oxide thermoelectric module for power generation measurement with eight *p*–*n* couples. One set module was arranged by two *p*–*n* couples with an alumina plate (32 mm × 32 mm × 1 mm) for hot bottom, and three alumina plate for cold top of the module (one in half size (32 mm × 15 mm × 1 mm) and two in a quarter size (18 mm × 15 mm × 1 mm)). The module shown in Fig. 1 is formed by four sets of modules, in which eight *p*–*n* couples were connected in series (each set comprised two *p*–*n* couples connected in series along with an electrode printed on the alumina plate; then, four sets of modules were connected in series using Ag wire). Further, all the three modules with different numbers of *p*–*n* couples were prepared: 8, 30, and 44.

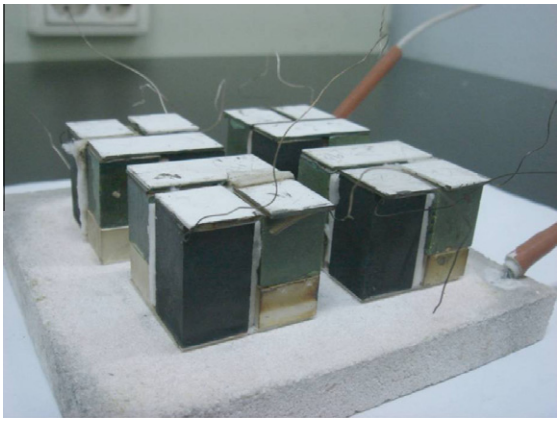

Fig. 1. Photograph of the oxide thermoelectric module for power generation measurements with eight *p*–*n* couples, taken after several power generation measurements.

To make the *p*–*n* couples, Ag-paste was initially printed on both the top and the bottom of each *p*-type $Ca_3Co_4O_9$ and *n*-type $(ZnO)_7In_2O_3$ leg. Ag-paste was also printed on the entire surface of the dummy electrode. Then, the Ag-paste for connecting the electrodes of the *p*–*n* couples was printed on the alumina plates for both the hot and cold parts by the screen printing method. For removing organics contained in the printed Ag-paste, all of these parts were dried in an oven at 150 °C. The Ag wires were bonded with Ag-paste to form series connections. Finally, the module was heat treated at 850 °C for 1 h under uniaxial pressure to create the contact between the legs and the electrodes.

2.3. Power generation characteristics of the TE module

The modules manufactured by the methods described above were placed over a hot plate, and a cooling fan was placed over the module to produce a temperature deviation in the module by compulsion. In order to measure the temperatures of both the hot and cold sides, two *k*-type thermocouples were placed at the point between the fan and the module and at the point between the module and the hot plate. The open circuit voltage and many other voltages at the condition of power generation were measured by a voltage meter. The power generation characteristics were measured by changing the external resistance of the circuit from ∞ to 0 with a source meter (Keithley 2420).

To optimize the efficiency of the module by maximizing temperature differences between the hot and the cold sides, the open spaces along with the sintered *p*- and *n*-legs were filled with calcined ceramic papers for adiabatic blocking. The differences between the power generation characteristics of modules with and without adiabatic block were contrasted. Fig. 2 shows images of the modules with and without adiabatic blocks. Finally, the electrical power generation characteristics were monitored by changing both the temperature conditions and the number of *p*–*n* couples required to generate maximum power.

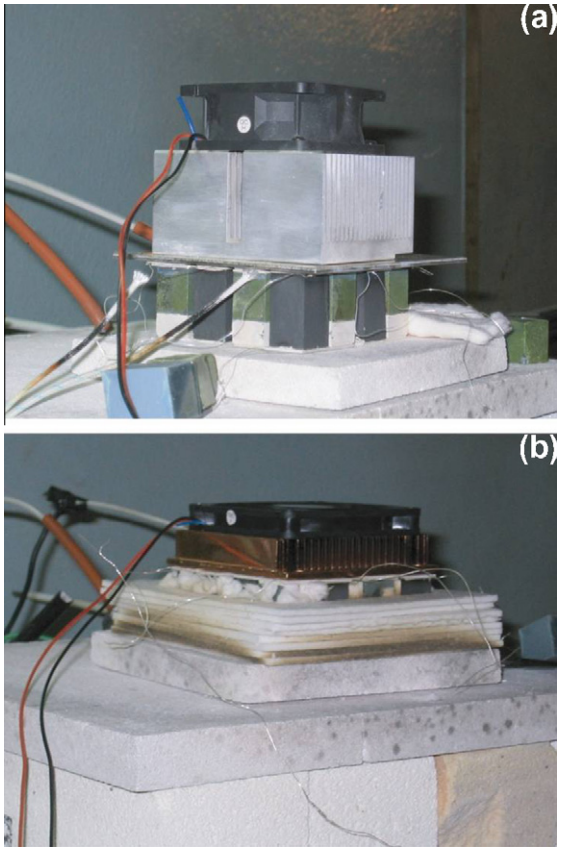

Fig. 2. Photographs of the module (a) with and (b) without adiabatic blocks.

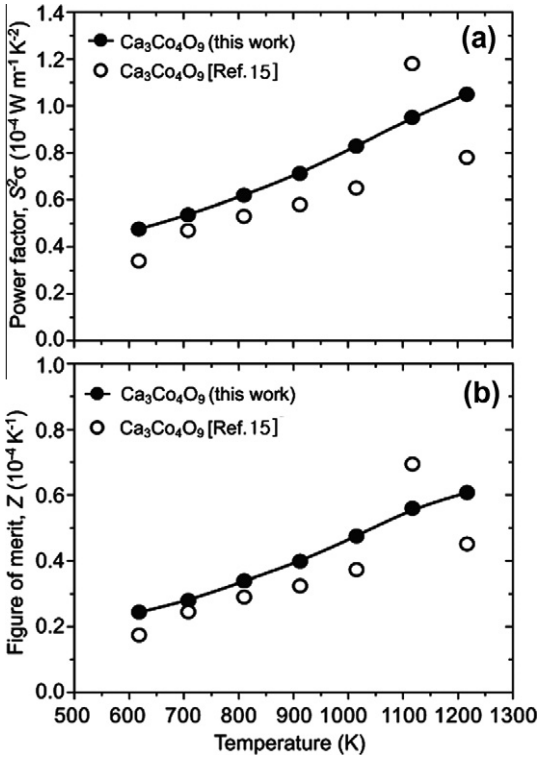

Fig. 3. Temperature dependence of (a) the power factor and (b) figure of merit (Z) for p-type $Ca_3Co_4O_9$ with textured structure. Open circles represent the data for $Ca_3Co_4O_9$ in Ref. [15]. The thermal conductivity values with temperature are shown in the inset of (a).

3. Results and discussion

Fig. 3 shows the temperature dependence of power factor ($S^2\sigma$) and the figure of merit (Z) for the p-type $Ca_3Co_4O_9$ leg. The inset of Fig. 3a shows the κ values with temperature. The values of $S^2\sigma$ and Z increase proportionally with temperature, and the observed behavior of the plot is similar to that of reported data [15], although the absolute values are a little higher the reported values. This observation implies that the TE properties of $Ca_3Co_4O_9$ layered structure are dominated by the degree of orientation. The observed $S^2\sigma$ and Z values at 1100 K were 0.9 W m^{-1} K^{-2} and 0.55 K^{-1}, respectively.

Fig. 4 shows the temperature dependence of $S^2\sigma$ and Z for the n-type $(ZnO)_7In_2O_3$ leg. The inset of Fig. 4a shows the κ values with temperature. The κ values of $(ZnO)_mIn_2O_3$ ($3 \leqslant m \leqslant 9$) polycrystalline samples are shown for comparison. As shown in Fig. 4a, the $S^2\sigma$ values showed little variation with m; however, the κ values significantly decreased with an increase in m. The maximum Z value could be obtained in $(ZnO)_7In_2O_3$ at all measured temperatures, and maximum power density is expected using $(ZnO)_7In_2O_3$ as n-type legs. It is noted that the Z value of $Ca_3Co_4O_9$ was smaller than that of $(ZnO)_7In_2O_3$ ($Z_{Ca_3Co_4O_9}$ at 1100 K $\sim$ 0.55 K^{-1}, $Z_{(ZnO)_7In_2O_3}$ at 1100 K $\sim$ 1.35 K^{-1}). This result implies that the TE performance of $Ca_3Co_4O_9$ should be enhanced by textured structure engineering to increase efficiency of the $Ca_3Co_4O_9$–$(ZnO)_7In_2O_3$ module.

Fig. 5 shows the power generation characteristics for the module comprising eight p–n couples at a temperature near 1050 K on the hot-side. Without the adiabatic blocks, the temperature on the hot-side (T_{hot}) and the cold-side (T_{cold}) were 1048 K and 512 K, respectively, and the temperature difference (ΔT) was 536 K. With the adiabatic blocks inserted into the modules, the temperature conditions were T_{hot} = 1023 K, T_{cold} = 365 K, and ΔT = 658 K. Under

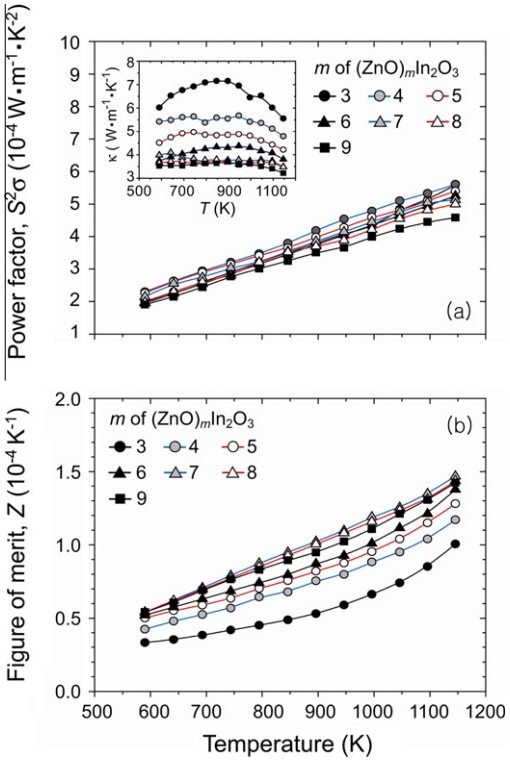

Fig. 4. Temperature dependence of (a) the power factor and (b) figure of merit (Z) for n-type $(ZnO)_mIn_2O_3$ ($1 \leqslant m \leqslant 9$) with textured structure. The thermal conductivity values with temperature are shown in the inset of (a).

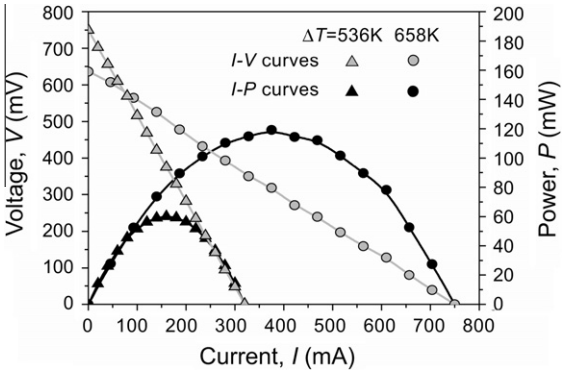

Fig. 5. Power generation characteristics of the module comprising eight *p*–*n* couples for hot-side temperature near 1050 K.

the same temperature conditions, the external resistance of the circuit was changed from $R = 0$ to ∞. As shown in Fig. 5, the open circuit voltage and the short circuit current (the current corresponding to $V = 0$) of the module were 760 mV and 320 mA under $\Delta T = 536$ K, and 640 mV and 750 mA under $\Delta T = 658$ K, respectively.

The maximum power output for modules with adiabatic blocks was 120 mW at $I = 375$ mA under $\Delta T = 658$ K, whereas for modules without adiabatic blocks, it was 60 mW at $I = 160$ mA under $\Delta T = 536$ K; these results indicate that the adiabatic blocks were essential to maintain the performance of the TE power generation source (ΔT).

The theoretical open circuit voltage (V_{cal}) for the module with adiabatic blocks could be expressed as

$$V_{cal} = (S_p - S_n) \times (T_{hot} - T_{cold}) \times n \quad (1)$$

where n is the number of couples. For the module comprising eight *p*–*n* couples, $V_{cal} = 1180$ mV was calculated ($S_p = 143\ \mu V\ K^{-1}$, $S_n = -82\ \mu V\ K^{-1}$, $T_{hot} - T_{cold} = 658$ K, $n = 8$); however, the measured open circuit voltage of 640 mV corresponds to only 54% of V_{cal}. This voltage loss could have originated from many factors including inhomogeneous temperature differences, unfavorable junctions between the TE legs and the electrodes, and contact resistance. Further research should be conducted on electrodes for *p*- and *n*-type legs and the design of the module to maximize thermal efficiency.

The power generation characteristics for varying temperature conditions and numbers of *p*–*n* couples were also investigated. Figs. 6 and 7 show the generated power of modules comprising 30 and 44 *p*–*n* couples, respectively. As shown in Fig. 6 the maximum power (P_{max}) increases with T_{hot}, leading to an increase in ΔT. The similarities have been reported as well some other systems [10,11] and supported also by a computational model [16]. The inset of Fig. 6 shows P_{max} with the number of *p*–*n* couples. Although the ΔT values are slightly different, P_{max} increases systematically with the number of *p*–*n* couples, indicating that TE power can be simply controlled by a change in module design. As shown in Fig. 7, the largest P_{max} value observed in this study, 423 mW, was obtained in a module with 44 *p*–*n* couples under the thermal condition of a hot-side temperature of 1100 K and a temperature difference of $\Delta T = 673$ K. The open circuit voltage of this module was 1800 mV. The durability and mechanical strength of the device were investigated by repeated operation of the module comprising 8 *p*–*n* couples under the thermal condition $T_{hot} \sim 1100$ K. The photograph shown in Fig. 1 was taken after several power generation measurements. Considering that the performance of the module was almost unchanged and the module was mechanically undamaged, the present module appears promising even for applications in the high-temperature region of up to 1100 K.

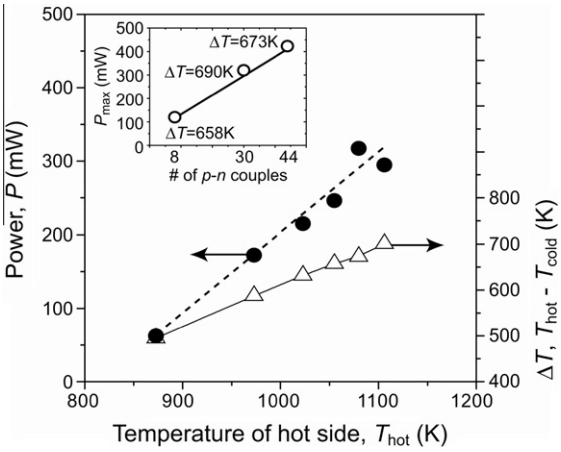

Fig. 6. The maximum power and temperature difference between hot and cold sides of the module comprising 30 *p*–*n* couples as a function of the hot-side temperature. The maximum power values with the number of *p*–*n* couples are shown in the inset.

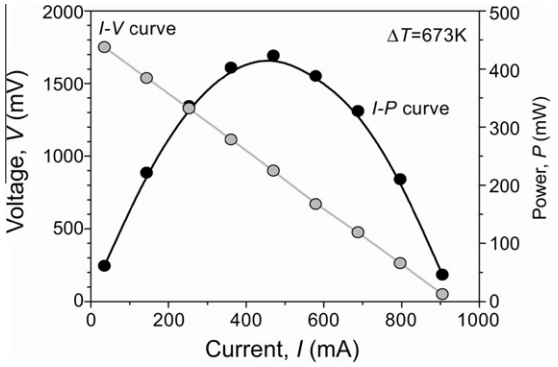

Fig. 7. Power generation characteristics of the module comprising 44 *p*–*n* couples for a hot-side temperature of 1100 K and a temperature difference of 673 K.

The performance of the module was compared with that of other the oxide-based modules developed thus far. Data listed in Table 1 are results from the module with *p*–*n* couples in a planer arrangement. The power generation results of the module with *p*-type $Ca_3Co_4O_9$ and *n*-type $(ZnO)_7In_2O_3$ couples have not been reported. Although simple comparison between the numerical values of P_{max} is difficult due to differences in the dimensions of *p*- and *n*-legs, the measured maximum power output (423 mW) of the present study is the largest value reported to date.

Overall, the following facts must be noted: (1) the measured open circuit voltage from the present modules was only 54% of the theoretical value, mainly due to voltage loss on the interfaces and the contact resistance, (2) the module was generated without the optimized electrodes, and (3) the microstructure of the present TE oxides was not finely controlled. Recently, the adverse effect of unfavorable junctions between legs and electrodes on TE power generation was reported by Funahashi and Urata [10]. They reported that the main factors responsible for the deterioration of module performance were dry joints, including pores, originating from the differences between the legs and the electrodes with regard to thermal expansion and/or poor affinity. The significant voltage loss in this study should be related to unfavorable contact between the legs and the electrodes. Future work will include improvement of the power generation performance of the module, not only by the reduction of contact loss but also by using materials with increased TE figures of merit. Precise study on the long term stability of the leg materials and electrodes for *p*- and *n*-type

Table 1
Thermal conditions, open circuit voltage V_0, and maximum output power P_{max} for reported oxides modules.

Ref. #	Materials	# of p–n couples	Element dimension (mm)	Joining technique	ΔT (K)	V_0 (V)	P_{max} (mW)	$P_{max}/\Delta T$ (mW/K)
[9]	p: $NaCo_2O_4$ n: ZnO	12		Diffusion welding	455	0.79	52.5	0.115
[10]	p: $Ca_{2.7}Bi_{0.3}Co_4O_9$ n: $La_{0.9}Bi_{0.1}NiO_3$	140	$1.3 \times 1.3 \times 5$	Ag-paste	551	4.5	150	0.272
[10]	p: $Ca_{2.7}Bi_{0.3}Co_4O_9$ n: $La_{0.9}Bi_{0.1}NiO_3$	8	3.7×4–4.5×4.7	Ag-paste	565	1	170	0.301
[8]	p: $Ca_{2.75}Gd_{0.25}Co_4O_9$ n: $Ca_{0.92}La_{0.08}MnO_3$	8	3×5–6×30	Pt-paste	390	0.988	63.5	0.163
This work	p: $Ca_3Co_4O_9$ n: $(ZnO)_7In_2O_3$	44	p: $15 \times 15 \times 27$ n: $15 \times 15 \times 18$	Ag-paste	673	1.8	423	0.629

oxides will also be reported. The findings of this study will be helpful in design for high density thermoelectric power generation system aiming at power generation utilizing waste heat in the high-temperature region.

4. Conclusions

A practical oxide-based thermoelectric module consisting of p-type $Ca_3Co_4O_9$ and n-type $(ZnO)_7In_2O_3$ sintered oxides has been successfully fabricated. It was found that adiabatic blocks are essential to maintain the temperature difference between the hot and the cold sides of the module. The maximum power of the module increases with the hot-side temperature, leading to an increase in the temperature difference. The maximum power increases systematically with the number of p–n couples. A maximum power output of 423 mW was achieved in the module with 44 p–n couples with a hot-side temperature of 1100 K and a temperature difference of 673 K.

Acknowledgment

This study was supported by the R&D Program for Energy and Resource funded by the Ministry of Knowledge Economy of the Korean Government.

References

[1] Rowe DM. CRC handbook of thermoelectrics. Boca Raton (FL): CRC Press; 1995.
[2] Miyazaki Y. Crystal structure and thermoelectric properties of the misfit-layered cobalt oxides. Solid State Ionics 2004;172:463–7.
[3] Prevel M, Lemonnier S, Klein Y, Hebert S, Chateigner D. Textured $Ca_3Co_4O_9$ thermoelectric oxides by thermoforging process. J Appl Phys 2005;98:093706.
[4] Liu Y, Lin Y, Shi Z, Nan CW, Shen Z. Preparation of $Ca_3Co_4O_9$ and improvement of its thermoelectric properties by spark plasma sintering. J Am Ceram Soc 2005;88:1337–40.
[5] Isobe S, Tani T, Masuda Y, Seo WS, Koumoto K. Thermoelectric performance of yttrium-substituted $(ZnO)_5In_2O_3$ improved through ceramic texturing. Jpn J Appl Phys 2002;41:731–2.
[6] Seo WS, Otsuka R, Okuno H, Koumoto K. Thermoelectric properties of Zn–In complex chalcogenides. In: Proceeding of the 17th international conference on thermoelectrics; 1998. p. 602–5.
[7] Noudem JG, Lemonnier S, Prevel M, Reddy ES, Guilmeau E, Goupil C. Thermoelectric ceramics for generators. J Eur Ceram Soc 2008;28:41–8.
[8] Matsubara I, Funahashi R, Takeuchi T, Sodeoka S, Shimizu T, Ueno K. Fabrication of an all-oxide thermoelectric power generator. Appl Phys Lett 2001;78:3627–9.
[9] Souma T, Ohtaki M, Ohnishi K, Shigeno M, Ohba Y, Shimozaki T. Power generation characteristics of oxide thermoelectric modules incorporating nanostructured ZnO sintered materials. In: Proceeding of the 26th international conference on thermoelectrics; 2007. p. 38–41.
[10] Funahashi R, Urata S. Fabrication and application of an oxide thermoelectric system. Int J Appl Ceram Technol 2007;4(4):297–307.
[11] Shin W, Murayama N, Ikdea K, Sago S. Thermoelectric power generation Li-doped NiO and (Ba, Sr) PbO_3 module. J Power Sources 2001;103:80–5.
[12] Masuda Y, Ohta M, Seo WS, Pitschke W, Koumoto K. Structure and thermoelectric transport properties of isoelectronically substituted $(ZnO)_5In_2O_3$. J Solid State Chem 2000;150:221–7.
[13] Kaga H, Asahi R, Tani T. Thermoelectric properties of highly textured Ca-doped $(ZnO)_mIn_2O_3$ ceramicsl. Jap J Appl Phys 2004;43(10):7133–6.
[14] Park KS, Kim KK, Seong JK, Kim SJ, Kim JG, Cho WS, et al. Improved thermoelectric properties by adding Al for Zn in $(ZnO)_mIn_2O_3$. Mater Lett 2007;61:4759–62.
[15] Li S, Funahashi R, Matsubara I, Yomada H, Ueno K, Sooleoka S. Synthesis and thermoelectric properties of the new oxide ceramics $Ca_{3-x}Sr_xCo_4O_{9+\delta}$ ($x = 0.0$–1.0). Ceram Int 2001;27:321–4.
[16] Rodriguez A, Vian JG, Astrain D, Martinez A. Study of thermoelectric systems applied to electric power generation. Energy Convers Manage 2009;50:1236–43.